Fuel Cell-based CHP System Modelling using Artificial Neural Networks aimed at developing Techno-Economic Efficiency maximization control systems

F.J. Asensio[a], J.I. San Martín[a*], I. Zamora[b], J. Garcia-Villalobos[b]

[a]Electrical Engineering Department, Engineering School of Gipuzkoa (Section of Eibar), University of the Basque Country UPV-EHU, Eibar 20600, Spain
[b]Electrical Engineering Department, Engineering School of Bilbao, University of the Basque Country UPV-EHU, Bilbao 48013, Spain

A B S T R A C T

This paper focuses on the modelling of the performance of a Polymer Electrolyte Membrane Fuel Cell (PEMFC)-based cogeneration system in order to integrate it in hybrid and/or connected to grid systems and analyse the techno-economic efficiency of the system in which it is integrated. To this end, experimental tests on a PEMFC-based cogeneration system of 600 W of electrical power have been performed in order to train an Artificial Neural Network (ANN). Once the learning of the ANN, it has been able to emulate real operating conditions, such as the cooling water out temperature and the hydrogen consumption of the PEMFC depending on several variables, such as the electric power demanded, temperature of the inlet water flow to the cooling circuit, cooling water flow and the heat demanded to the CHP system. After analysing the results, it is concluded that the presented model reproduces with sufficient accuracy and precision the performance of the experimented PEMFC, thus enabling the use of the model and the ANN learning and implementation methodology presented in this work in order to model other PEMFC-based cogeneration systems and integrate them in techno-economic efficiency optimization control systems.

.

1. Introduction

The modelling of Polymer Electrolyte Membrane Fuel Cell (PEMFC) systems that emulate exactly its operation is an important aspect when studying operational strategies, its integration with other systems or evaluation of control algorithms that aim to maximize the energy efficiency of the system [1], [2], [3].

Currently there are several models of PEMFC which reproduce with sufficient accuracy the dynamic characteristics and its behaviour in the steady state [4], [5], [6]. However, in current literature there is little information available regarding PEMFC models that emulate their behaviour when they are integrated into cogeneration systems, in which, besides taking into account the intrinsic characteristics of the PEMFC, they must take into account the characteristics of the entire system that integrates them and affect their operation, such as the heat extracted from the PEMFC by the cooling circuit. In this context, in [7], [8] and [9], PEMFC models that are capable of emulating the thermal behaviour of them in order to study their integration into a Combined Heat and Power (CHP) system are shown. However, most of the developed models are analytical. The development of this type of models is very complex due to the relationships between the variables involved in this. In addition, some of the necessary variables for the implementation of this type of models are difficult to calculate and it is therefore necessary to use approximations, which must be adjusted empirically [9].

The setting of these unknown variables by experimental methods requires a great effort and sometimes it is difficult to get sufficient accuracy in the model using this technique. In this sense, the implementation of an empirical model of PEMFC-based cogeneration system using Artificial Neural Networks (ANNs) enables the study of these systems in an easy and accurate manner, without the need for complex analytical models in which is indispensable to know the intrinsic characteristics of the system [10].

In the context of ANN-based modelling, there can be found several works in which models aimed at simulating the performance of a PEMFC are developed [10], [11], [12], [13], [14], [15], [16], [17], [18], [19]. However, almost all focus on the electrical behaviour and, the temperature of the system, is taken into account as an input variable instead of taken it as an output variable. I.S. Han et al., propose a model in which the cathode temperature of a PEMFC is obtained as an output variable with good accuracy, however, the hydrogen consumption rate is not considered in the model [20]. A.U. Chavez-Ramirez et al. and G. Napoli et al., propose a model that also provides the cathode temperature with good accuracy, but they set the flow rate of hydrogen consumed as an input variable to the model instead of an output variable [21], [22]. In-Su Han et al., present a fuel cell model in which the temperature of the outlet cooling fluid is obtained by a neural network and they also contemplate the hydrogen consumption, however, this is obtained by a semi-empirical relationship in which hydrogen flow rate is linearly related to output current, thus, not contemplating the system temperature in the relationship [23].

Hydrogen flow rate consumed by a fuel cell and the efficiency thereof, depends, among other factors, on the electrical and thermal power generated by the stack. Due to the complex dynamics of internal relations that define the behaviour of a fuel cell, it is difficult to know beforehand with precision the flow of hydrogen consumed, so that in order to analyse the efficiency of the system, it becomes essential to know the flow consumed in real operating conditions.

Generally, in PEMFC systems that include a cooling circuit by forced circulation of liquid, the temperature of the stack is controlled in order to maintain it at a constant value, so that the amount of heat extracted from the fuel cell is directly linked to the regulation of temperature. In a CHP system based on PEMFC, provided that the operating temperature limits are not exceeded, the heat extracted from the stack can also be linked to the heat demand and not just to the temperature regulation. Under these conditions, heat extracted must be taken into account as an external variable, independently of the PEMFC temperature control, which is a key factor to study the effect of variations in thermal demand on system efficiency.

The model developed in this paper is able to provide, accurately, the flow of hydrogen consumed and the outlet temperature of the coolant fluid of the PEMFC, not only in terms of electrical output, but also in terms of variations in the heat demand of the system. This aspect, allows integrating the model obtained in hybrid systems and / or connected to the grid, with time-based electricity rates, in which control strategies aimed at maximizing the global techno-economic efficiency of the system are applied, since, it is possible to predict at any time the electrical

and thermal efficiency, and therefore the fuel cell generation cost versus the cost of other sources of electricity and heat generation, and based thereon, determine the optimum system performance.

2. Experimental Analysis

2.1. Equipment used

Fig. 1 shows the HP600 PEMFC-based CHP system used in this work, which consists of a PEMFC of 600 W of electric power and a cooling system based on a forced-convection heat exchanger, which can be controlled in order to change the heat demand of the system.
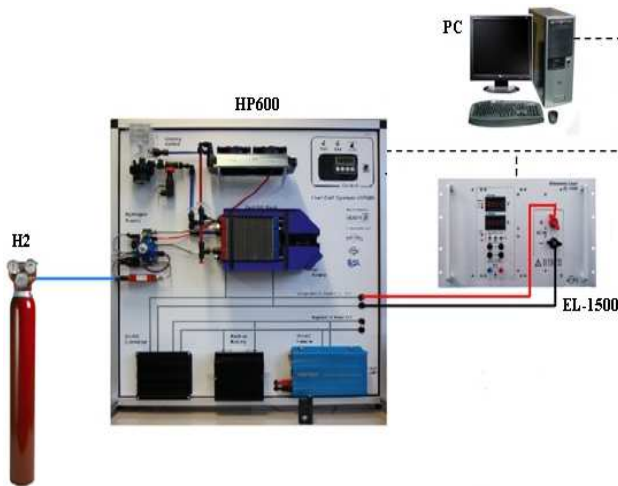

Fig. 1. Arrangement of the equipment for testing.

In addition to the fuel cell stack and the cooling system, the HP600 has a power conditioning system that comprises a DC / DC converter, lead acid battery and a power inverter. However, they have not been used to carrying out the tests presented in this paper, since the proposed model is focused only on the energy performance of the fuel cell stack.

To establish and control the electricity demand, it has been used the programmable electronic load EL-1500, which has been connected directly to the output terminals of the fuel cell stack, after the derivation for the auxiliary equipment.

The energy source of the system is based on a 50 litres bottle of pressurized hydrogen stored at 200 bar.

Table 1 shows the most relevant technical characteristics of the HP600 PEMFC-based CHP system.

Table 1
Technical characteristics of the HP600 system.

Parameter	Value
DC unregulated output voltage	13.5 - 22 V_{DC}
Rated current	45 A
Rated voltage	14.4 V
Short-circuit voltage	23.5V
Rated hydrogen pressure	4-8 bar (regulated by pressure gauge)
Ambient operation temperature range	15 - 35°C
Operation temperature	45 - 60°C
Active area	24 cells, 130cm^2 each
Cooling fluid	Demineralized water (conductivity < 1uS/cm)
Hydrogen purity	>4.0 (99.99% of purity) or hydrogen 3.0 from electrolyser (not allowed sulfur compounds and other poisonous parts)
Hydrogen flow rate @ Rated power	9 SLPM

2.2. Data acquisition

In the tests, variations in the demand of the electric and thermal power of the PEMFC have been done, observing the response of various parameters of it, such as the stack voltage, stack current, generated electric power, generated heat, hydrogen flow rate, water flow in the cooling circuit, water inlet and outlet temperature in the cooling circuit, stack temperature, etc.

To obtain the instantaneous values of the magnitudes, it has been used a program developed in LabVIEW environment.

Additionally, other program in LabVIEW environment has been created in order to control the EL-1500 programmable electronic load.

In order to emulate the system efficiency over the time and the thermal inertia with the highest possible reliability, it has been established the sampling time of data acquired in one sample per second.

All data have been exported to an excel spreadsheet for further interpretation, study and use in the training process of the ANN.

2.3. Energy demand load profiles

When choosing the load profile with which the tests have to be carried out, it is essential to consider the purpose for which the model is intended, which in this case is the development of a model that can simulate the performance of a PEMFC-based CHP system in order to predict the electrical and thermal efficiency of the system depending on the electrical and thermal energy demand. In this sense, both heat and electric demand profiles have been created, considering that the amount of thermal energy extracted from the stack can vary for different demands of electrical power, always within the range within fuel cell is capable of supplying.

Fig. 2 shows the thermal and electrical profiles created in order to acquire the necessary values to train the ANN.
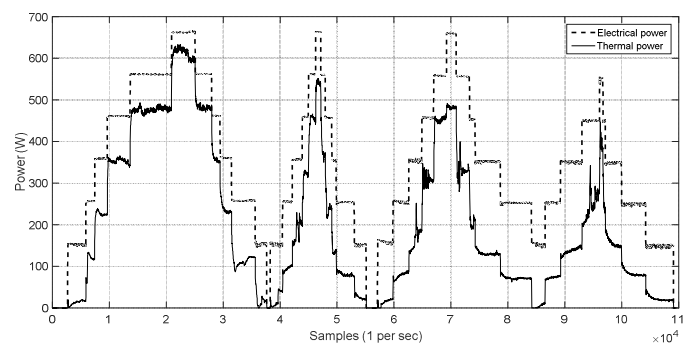

Fig. 2. Electrical and thermal load profiles.

As can be seen in Fig. 2, when the PEMFC system is generating certain electrical power, not necessarily always it has been demanded the same thermal power. In this way, it is considered a variation in the thermal demand regardless of electrical power demand. Besides, it has to be noted that the thermal demand must be controlled within a range so that the limits of the operating temperature of the PEMFC are not exceed.

2.4. Experimental Results

Table 2 shows the ranges of most important magnitudes achieved during the test.

Table 2
Technical characteristics of the HP600 system.

Magnitude	Range	Units
Electrical power	[0 – 667.5]	[W]
Thermal Power	[0 – 633.1]	[W]
Stack voltage	[13.01 – 19.86]	[V]
Stack current	[0 – 49.82]	[A]
Hydrogen flow rate	[0.14 – 8.32]	[SLPM]
Water inlet temperature	[16.02 – 61.58]	[ºC]
Water outlet temperature	[16.02 – 67]	[ºC]
Water flow	[0.99 – 1.1]	[l/min]

Table 2 shows that although the minimum demanded electric power has been of 0 W, the minimum hydrogen flow rate has not been zero. This minimum consumption is due to the consumption of auxiliary elements of the PEMFC system, such as the control system, water pump or air compressor. In this sense, since the hydrogen flow rate contemplates implicitly the consumption of these devices, it has been achieved a model that can also represent the consumption of the control and regulation system of the fuel cell itself, which is fundamental when calculating the whole system efficiency.

Fig. 3 shows the electrical power provided and the hydrogen consumed by the PEMFC (up) and its voltage and current (down).
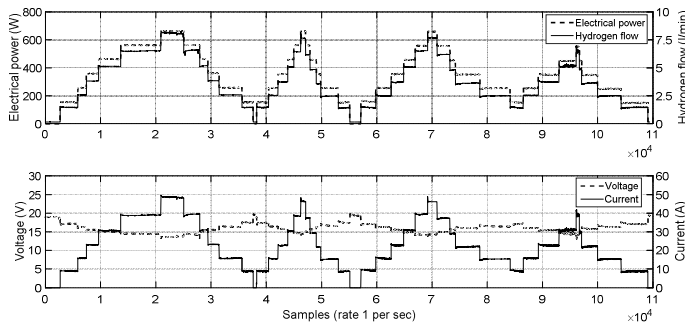
Fig. 3. Electrical power and hydrogen consumed (up) and stack voltage and current (down) during the test.

During the test, it has been found that for the same electric power demand, different hydrogen flow rates have been measured. For example, for an electrical power of about 150 W, it has been obtained a maximum relative difference between hydrogen consumptions of 6.12%, with a maximum consumption of 1.47 slpm (standard litres per minute) at a stack temperature of 20.79 °C, and a minimum consumption of 1.38 slpm, at a stack temperature of 40.32 °C.

This effect is related to temperature of the stack, since the hotter is the fuel cell, i.e., when it is extracted less heat, the more is increased the speed of the catalytic reactions, which in turn leads to higher electrical efficiency and therefore lower consumption of hydrogen for the same electrical power generated. In Fig. 5 it can be shown this effect on the electrical efficiency of the PEMFC system.

Fig. 4 shows the thermal power and the water flow (up) and the temperature of the inlet and outlet water flow to the cooling circuit (down). It can be seen that as the heat demand is reduced, the coolant temperature is increased in temperature and, conversely, the higher is the heat demand, the lower is the coolant temperature at the outlet of the stack, and the greater is the temperature difference between inlet and outlet of the cooling circuit of the stack, thereby increasing the thermal efficiency of the system.
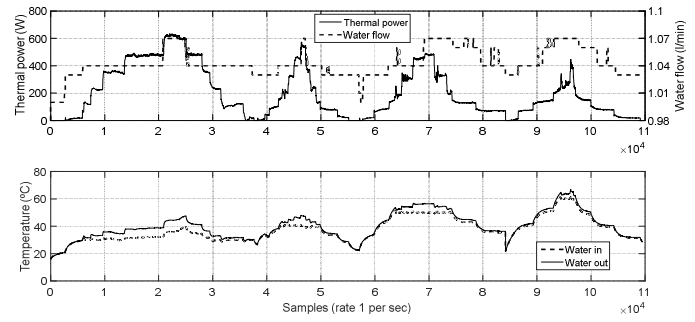
Fig. 4. Thermal power and water flow (up) and temperature of inlet water and outlet water of the cooling circuit (down) during the test.

Fig 5. shows the electrical, thermal and overall efficiency of the PEMFC-based CHP system obtained during the test.
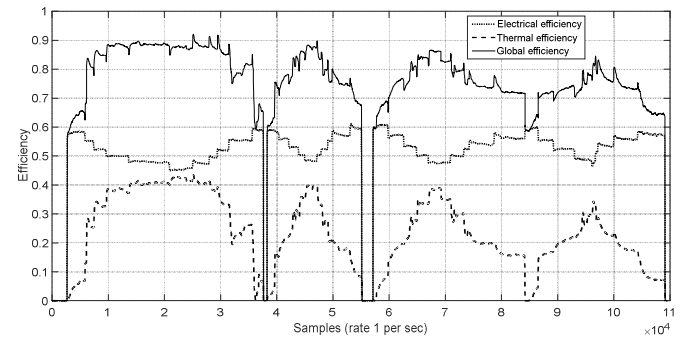
Fig. 5. Electrical, thermal and overall efficiency of the system during the test.

In Fig 5. it can be seen that electrical efficiency is decreased as thermal efficiency increases, resulting in greater overall efficiency. It has been achieved a maximum electrical and thermal efficiency of 61.11% and 43.43%, respectively. The overall efficiency achieved during the test has been of 91.8%. However, it must be taken into account that, despite it is considered the power consumption of system management and control system itself, power conditioning devices have not been considered, so that if power converters were integrated, electrical and overall efficiency obtained would be reduced slightly.

3. Implementation and training of the ANN

3.1. Architecture of the Neuronal Network

Due to the high nonlinearity of system to be modelled and the time-dependence of the target variables to be calculated, an autoregressive with exogenous inputs (NARX)-based feedback neural network has been implemented for calculating the stack cooling water out temperature and the hydrogen consumption of the PEMFC-based CHP system, since such architectures become a good solution when it comes to systems with thermal inertia and non-linear behaviour [24].

A feedback NARX network is a recurrent dynamic network, with feedback connections forming a loop where information back from front to back. This network takes as input variables both exogenous variables and their delays and the delays of the output signals themselves provided by the network. In Fig 6. it is shown the general scheme of a two-layer feedback NARX network.
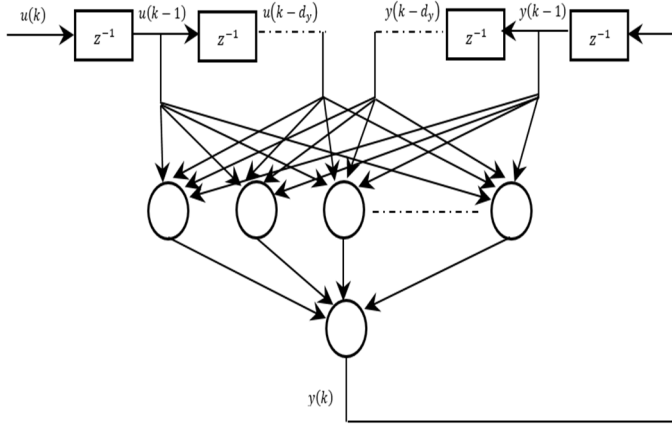
Fig. 6. Architecture of a tow-layer feedback NARX network.

Equation (1) shows the output provided by the neural network.

$$y(k) = f\left(u(k-1), \dots, u(k-d_u), y(k-1), \dots, y(k-d_y)\right) \qquad (1)$$

Where $y(k)$ is the value of the time series to be predicted at time step k and, $u(k)$ is the set of exogenous input variables at time step k. The terms $u(k-1), \dots, u(k-d_u)$ and $y(k-1), \dots, y(k-d_y)$ represent the delays of both variables the exogenous inputs and endogenous outputs between time step k and the time steps d_u and d_y respectively. $f()$ is the nonlinear mapping function to be implemented.

In this paper, has been taken the same delay order for both exogenous inputs and endogenous outputs ($d_u = d_y$).

In theory, the architecture of a NARX neural network allows the implementation of infinite configurations, varying the number of layers and the number of neurons per layer. Although still has not been demonstrated the optimal number of layers and neurons that has to be used for each application, it can be associated the number of these with the complexity of the system to be modelled and the generalization ability of the neural network. If the neural network is very complex, i.e., having a high number of layers and neurons, therefore large number of free parameters (weights and biases), it will likely overfit the training data [25]. When this occurs, despite having shown good behaviour with the data with which has been trained, it may not show a good response with a new set of input data. In this sense, the simpler the neural network is and the lower number of weights and biases it uses, greater will be its ability to generalize and better behave will have facing a new data set.

In order to limit the number of weights and biases and avoid as far as possible the training data overfit, it has been limited the number of layers of the neural network to 2 layers: a hidden layer and an output layer.

The number of neurons in the output layer is determined by the number of target variables to be calculated, which in this case are two. Regarding to the number of neurons in the hidden layer, and the delay order of the inputs and outputs of the ANN, they have been established in 5 and 2, respectively. The optimum selection of these parameters is discussed in *section 3.3* of this paper.

Fig. 7 shows the final configuration of the NARX network used. It must be highlighted that the architecture shown corresponds to a series-parallel architecture used in the training process, where the real targets are used instead of the feedback

of the estimated outputs. Despite it does not include the feedback of the output, once the ANN has been trained, the output has been connected to the input, obtaining a parallel NARX architecture. The advantage of doing this is that the data used to train the network is more accurate than the one that would be used in case of taking into account the feedback of the output data during the training process [26].

3.2.   Data pre-processing

Hydrogen flow consumed and outlet temperature of the cooling fluid are established as targets, since with these two variables it is enough to evaluate the electrical and thermal efficiency of the PEMFC system, depending on the selected input variables, which are mentioned below.

After analysing the experimental results, the variables that are unrelated or indirectly related to the target variables are discarded, and are selected as input variables those variables that are directly related to targets. In this sense, there have been selected four input variables: inlet temperature of the cooling fluid, flow rate of the cooling fluid, and electric and thermal power demanded from the PEMFC system.

Once selected the input and output variables, it has been proceeded to its treatment to facilitate the process of training of the neural network.

As can be seen in Fig. 7, each net input is a product of the corresponding input times the weight plus the bias. Since the symmetric sigmoid transfer function is used in the hidden layer, if the input is very large at the beginning of the training process, then the applied weight has to be very small in order to avoid the saturation of the mentioned transfer function, and therefore, the gradient will be very small too. To avoid this situation, both inputs and outputs have been normalized so that all the data is within the range -1 to 1.

In equation (2) it is shown the procedure to normalize the data as above mentioned.

$$p = 2(u - u^{min})./(u^{max} - u^{min}) - 1 \qquad (2)$$

Where u^{min} and u^{max} are the vectors containing the minimum and maximum values, respectively, of the input vectors u of the input data set, and p represents the resulting normalized input vectors.

The same normalization procedure shown in equation (2) is applied to the target vectors. After calculating the estimated outputs of the neural network, an inverse procedure is applied in order to obtain the magnitudes in the real scale.

In order to collect the largest possible number of different operating points, there have acquired a total of 109.466 samples per variable (6x109,466), which in turn have been separated into three blocks: 70% of the samples has been used for the training process; 15% has been used for testing process in order to estimating the generalization errors and detect possible poor generalization; the remaining 15%, has been used in the validation tests to prevent inefficient use of the neural network parameters and reduce the complexity of the same.

Finally, normalized vectors corresponding to each block are sequentially organized according to equation (2), by columns in matrix form, for their subsequent use in the process of training, testing and validation.
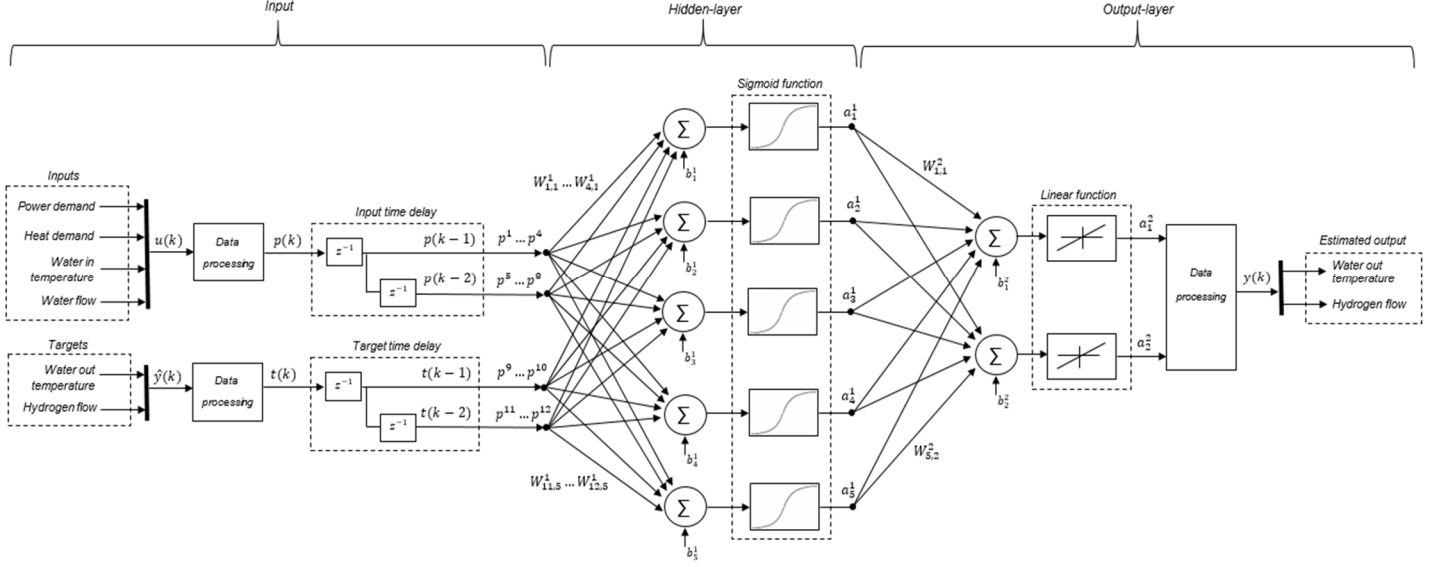
Fig. 7. **Series-parallel architecture of the implemented NARX**

3.3. Training process

On the basis of the diagram of Fig. 7, the network output a_i^{n+1} of each i neuron and N layer is obtained according to equation (3), given as:

$$a_i^{n+1} = f^{n+1}\left(\left(\sum_{j=1}^{k} W_{j,i}^{n+1} \cdot a_j^n\right) + b_i^{n+1}\right) \; for \; \begin{cases} n = 0, 1, \dots, L-1 \\ i = 1, 2, \dots, I \\ k = 1, 2, \dots, K \end{cases} \quad (3)$$

where L is the number of layer in the network, I is the number of neurons of the Lth layer, K is the number of inputs of the ith neuron of the Lth layer, $W_{j,i}^{n+1}$ is de weight applied to each jth input of the ith neuron, a_j^n is the output preceding the jth input, b_i^{n+1} is the bias applied to the ith neuron, and f^{n+1} is the mapping function used in the Lth layer.

Equation (4) shows the mapping function of the hidden-layer ($L = 1$), which is a symmetric sigmoid function, given as:

$$f(x) = \frac{2}{1 + e^{-2x}} - 1 \quad (4)$$

The mapping function of the output-layer ($L = 2$) is a linear function with gain 1.

In order to give a starting point to equation (3), in equation (5) it is shown the mapping of external inputs to the inputs of the neurons of the first layer, given as:

$$a_j^0 = p^j \quad (5)$$

The outputs of the network are the outputs of the last layer a^L.

In order to adjust the network weights and biases the Mean Squared Error (MSE) is used as performance index. Equation (6) shows the performance index, given as:

$$F(x(k)) = MSE = \frac{1}{N}\sum_{i=1}^{N}(t_i - a_i)^2 \quad (6)$$

where, N is the total samples of the training set, t_i represents the target values, a_i represents the network output values, and $x(k)$ is the vector containing all the network weights and biases at time step k.

Equation (7) and (8) show the calculation of the new weights and biases in each time step, given as:

$$W_{j,i}^L(k+1) = W_{j,i}^L(k) - \alpha(k)\frac{\partial F(x(k))}{\partial W_{j,i}^L} \quad (7)$$

$$b_i^L(k+1) = b_i^L(k) - \alpha(k)\frac{\partial F(x(k))}{\partial b_i^L} \quad (8)$$

where $\alpha(k)$ is the learning rate in each time step k, which is decreased in each step when the performance index has been reduced and, conversely, increased when the SME has grown.

In order to compute the equations (7) and (8), the *Levenberg-Manquardt* algorithm is used [27]. In the following *section 3.4* it is discussed the method used to stop the training in order to avoid the inefficient use of the parameters involved, thereby enabling the choice of the optimal neural network configuration.

3.4. Generalization improvement: choosing the optimal configuration

In the current literature, several authors have proposed different methods to establish the optimal number of neurons in the hidden layer, as well as the delay taps [25], [28], [29]. Among the most commonly used growing, pruning, comprehensive searches, regularization and early stopping are used [28]. However, it is difficult to determine the optimal number of neurons in the hidden layer, and often, this depends on the type of application and the level of complexity of the system to be

modelled. In this paper it has been used a cross-validation using as target function to minimize the Mean Squared Error (MSE).

In the context of cross-validation, there are several methods to determine the optimal configuration of the network during the training process.

In this paper, it has been used the method of early stopping, since it is one of the simplest methods to implement and in turn provides good results [30].

The early stopping method consists on deciding, in an efficiently manner, when to stop the training of the neural network. Since during the training process, as iterations elapse, more and more weights and biases could be used until a minimum pre-set error is achieved, the more iterations are computed the greater will be the complexity of the resulting network. In this sense, if training is stopped before the minimum error is reached, the equivalent neuronal network will be using fewer parameters and it will less likely to overfit [31].

To implement the early stopping, the validation set and the training set that previously have been separated from the entire data set are used.

While the training set is used to calculate the weights and biases during the training process, the validation set is used to monitor the behaviour of the network in each epoch. In that sense, every time the weights and biases are adjusted, the MSE is calculated using the validation set and, when the MSE obtained is increased consecutively for 6 epochs, it is ended the iterative process, obtaining as final result the weights and biases corresponding to the minimum MSE obtained with the validation set.

This process has been carried out for various configurations of neural network, varying the number of neurons in the hidden layer from 2 to 6, and the number of delays applied to the input and output variables from 1 to 3. In order to check how responds each neural network configuration to a new data set, it has been used the previously separated test set from the total data set, and then it has been calculated the MSE again for each configuration. Thus, it has been possible to determine which configuration has behaved more effectively, so that, it has been chosen as optimal, that configuration with the lowest MSE during the test, thus improving the generalization ability of the neural network obtained.

Table 3 shows the results obtained during the training, validation and test processes, for each neural network configuration implemented.

Table 3
Results obtained for different configurations during the training, validation and test processes.

Delay taps	Hidden neurons	Mean Squared Error (MSE)		
		Training	Validation	Test
1	2	4.48386e-4	3.93013e-4	5.51205e-4
1	3	4.18698e-4	6.62509e-4	4.98378e-4
1	4	4.00177e-4	5.37536e-4	4.59371e-4
1	5	4.33293e-4	5.35228e-4	4.20937e-4
1	6	3.89737e-4	3.72719e-4	5.69641e-4
2	2	3.48840e-4	4.33646e-4	4.61630e-4
2	3	3.67112e-4	4.09019e-4	3.80890e-4
2	4	3.72891e-4	4.38660e-4	3.14123e-4
2	5	3.53212e-4	2.20046e-4	2.87876e-4
2	6	3.62272e-4	4.00256e-4	4.29211e-4
3	2	3.86636e-4	3.35024e-4	3.20505e-4
3	3	3.69205e-4	3.76850e-4	3.49453e-4
3	4	3.31622e-4	4.96646e-4	3.81646e-4
3	5	3.13994e-4	4.77400e-4	3.83548e-4
3	6	3.53062e-4	3.47515e-4	3.85005e-4

It has been proven that the minimum MSE has been obtained with the configuration that includes 5 neurons in the hidden layer

and two delay taps applied to the input and output variables of the neural network. This configuration has been obtained after 46 epochs.

For the case in which there are used 1 and 2 delay taps, the more neurons in the hidden layer are used the more is decreased the MSE, till neuron 5 is reached, from which an error increase has been obtained. For the case in which three delay taps are used, the MSE has increased as more neurons are included in the hidden layer.

In addition to the MSE, as indicative of the effectiveness of the neural network, it has also been calculated regression between estimated outputs by the neural network and the targets, also obtaining the errors of the parameters that define the regression itself. Equation (9) shows the linear function to be adjusted, given as:

$$a_i = mt_i + b \tag{9}$$

where m is and b are the slope and offset of the linear function, respectively and, a_i and t_i, are the network outputs and targets, respectively.

The equations (10) and (11) show the calculation of the parameters of equation (9).

$$m = \frac{n \sum_{i=1}^{n}(t_i \cdot a_i) - (\sum_{i=1}^{n} t_i) \cdot (\sum_{i=1}^{n} a_i)}{n \sum_{i=1}^{n}(t_i{}^2) - (\sum_{i=1}^{n} t_i)^2} \tag{10}$$

$$b = \frac{n \sum_{i=1}^{n} a_i - m \sum_{i=1}^{n} t_i}{n} \tag{11}$$

Where n represents the total samples used. Equations (12) and (13) show the calculation of the slope error Δm and the offset error Δb.

$$\Delta m = \frac{\sqrt{n} \cdot \sqrt{\frac{\sum_{i=1}^{n}(a_i - mt_i - b)^2}{n-2}}}{\sqrt{n \sum_{i=1}^{n}(t_i{}^2) - (\sum_{i=1}^{n} t_i)^2}} \tag{12}$$

$$\Delta b = \Delta m \sqrt{\frac{\sum_{i=1}^{n}(t_i{}^2)}{n}} \tag{13}$$

Besides, in order to study the degree of dependence between the values estimated by the neural network and the real values, the correlation coefficient R has been calculated by means of equation (14), given as:

$$R = \frac{\sum_{i=1}^{n}(t_i - \langle t \rangle) \cdot (a_i - \langle a \rangle)}{\sqrt{\sum_{i=1}^{n}(t_i - \langle t \rangle)^2} \sqrt{\sum_{i=1}^{n}(a_i - \langle a \rangle)^2}} \tag{14}$$

In Fig. 8 and 9 the regression lines corresponding to the results obtained during the training and test processes for the target variables coolant temperature output and hydrogen consumed, respectively, are shown.
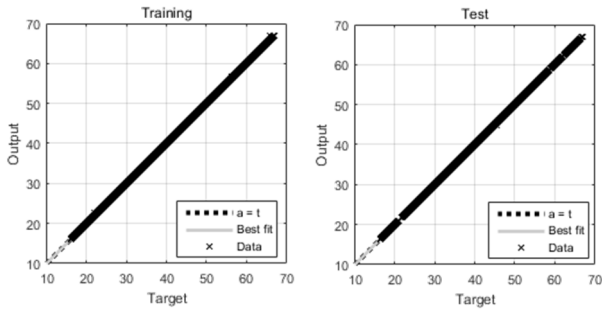
Fig. 8. Correlation of cooling water outlet temperature by linear regression for training (left) and testing (right).
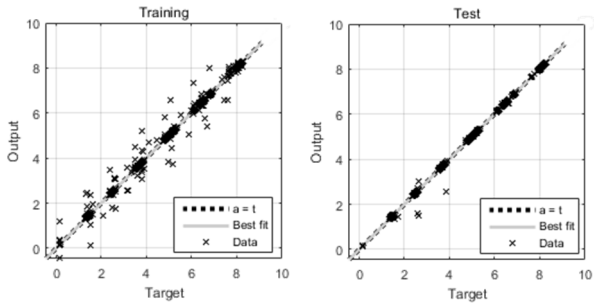

Fig. 9. Correlation of hydrogen flow rate by linear regression for training (left) and testing (right).

Table 3 shows the coefficients of the regression obtained from the test case for both variables the cooling water outlet temperature and the hydrogen flow consumed. As it can be seen, the slopes obtained are very close to unity and the offset are quite low.

Table 3
Regression coefficients for the testing case.

Variables	Slope m	Offset b	Slope error Δm	Offset error Δb	Correlation R
Outlet temp.	0.9986	0.0486	3.4e-05	1.4e-03	0.9999
h_2 flow rate	0.9900	0.0286	1.5e-04	6.6e-04	0.9987

4. Simulation results and discussion

Fig. 10 and 11 show the simulation results of the hydrogen flow rate and temperature of the outlet water flow, respectively, compared to the experimental results after training the optimal neural network with the 70 % of the total data obtained from the experimental test.
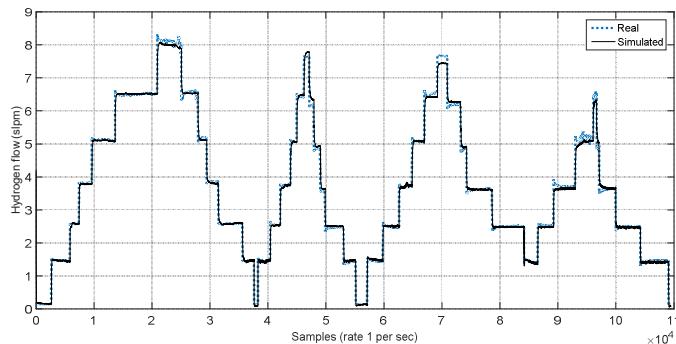

Fig. 10. Simulated and real hydrogen flow consumed.

As can be seen in Figure 10, simulation results show that the modeled system is capable of emulating quite accurately the hydrogen flow consumed by the PEMFC-based system, in which it is included the corresponding consumption of the system management and control devices. The maximum hydrogen flow rate deviation has been of 0.152 litres per minute, having given when the real hydrogen flow consumption was 6.19 litres per minute. This small deviation in the hydrogen flow has led to a maximum relative error of 2.45 % in the electrical efficiency simulated (Fig. 11), when the electrical and thermal power demands were of 560 W and 370.3 W, respectively, and the real electrical efficiency was of
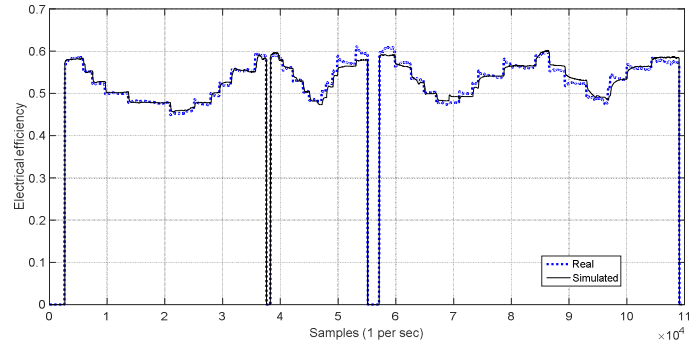

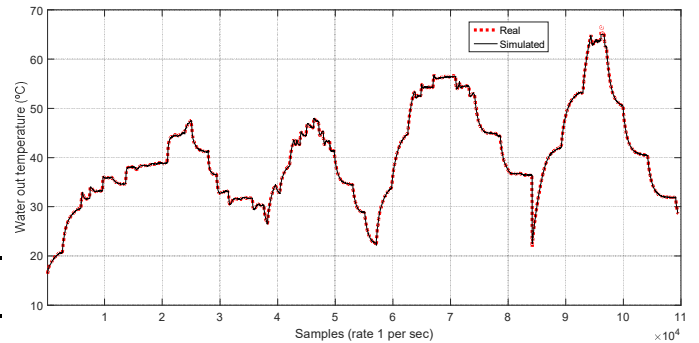**Fig. 11.** Simulated and real electrical efficiency of the system.

Fig. 12. Simulated and real temperature of the outlet water flow.

Regarding the simulation results of the temperature of the cooling outlet flow water obtained in the experimental test (Fig. 12), the maximum temperature deviation obtained between the experimental and simulated results has been of 2 ºC, having given this maximum deviation when the experimental temperature has reached its maximum value of 67 ºC. In most of the operating points analysed, the error obtained in the temperature has decreased in the same order in which the temperature has decreased.

In order to see how it affects the error of the temperature of the outlet flow in the estimated thermal efficiency (Fig. 13), it must be taken into account the error obtained when simulating the hydrogen consumption, since in the calculation of the thermal efficiency, both variables are involved. In this sense, the maximum relative error obtained in the thermal efficiency has been of 4.27 %, which has been produced in the same operating point in which the maximum deviation of the temperature of the outlet flow has been reached, when the electrical and thermal power demands were of 538.6 W and 435.5 W, respectively, and the real thermal efficiency was of 34,15 %.
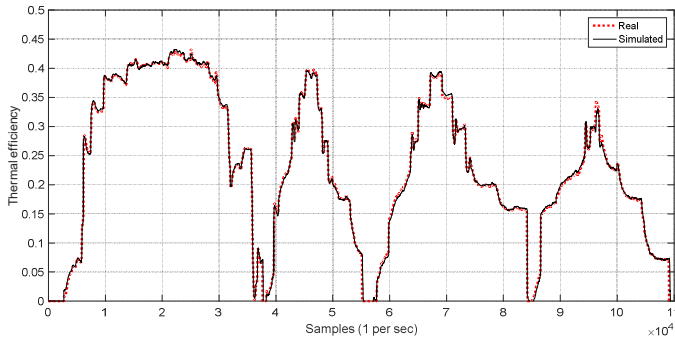
Fig. 13. Simulated and real thermal efficiency of the system.

Regarding the simulation results of the global efficiency of the PEMFC-based system (Fig. 14), if there are taken into account the errors of both curves the electrical efficiency and thermal efficiency, the maximum relative error obtained has been of 6.13 %, having given when the real global efficiency was of 80.12 %. The proportion of the contribution to this error by the electrical and thermal efficiency errors has been of 72,7 % and 27,3 %, respectively.
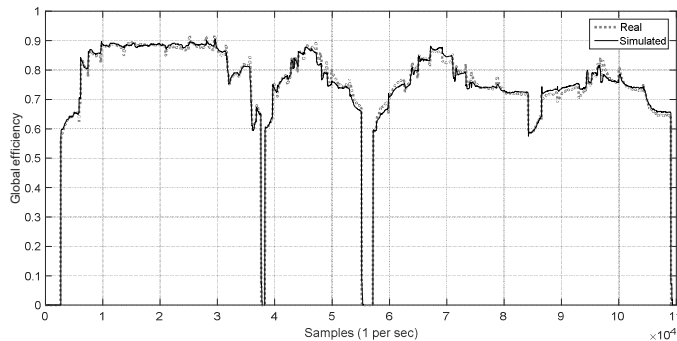

Fig. 14. Simulated and real global efficiency of the system.

The maximum absolute difference in the overall system efficiency obtained by the neural network, between operating points at same rated power, has been of 4.55% (89.05% - 84.5%), being the maximum difference obtained with the real data set of 8.91% (91.8% - 82.89%). Moreover, in these operating points have been obtained two maximum proportions regarding to the proportions of electrical and thermal efficiency simulated, which have been of 46.69% and 42.36% (real: 48.6% and 43.20%), and 49.23% and 35.27% (real: 48.17% and 34.72%), respectively.

Therefore, having obtained these differences in the efficiency of the system for the same electrical power and different thermal power demanded, it is shown the potential of these systems to be managed optimally, depending on energy needs, giving priority to the maximization of the electrical or thermal efficiency, depending on the generation costs of all devices involved in the system.

As an example, assuming that the PEMFC-based CHP system is integrated into a building which has access to the electrical grid and has an auxiliary system for heat generation, when there is a combined demand of electrical and thermal energy and, the sum of the costs of the energy consumed from the grid and the heat generation auxiliary system is greater than the cost of combined generation of heat and power derived from the PEMFC, but only the cost of the electricity is higher if it is produced by the PEMFC rather than if it is consumed from the grid, it will be worthwhile to extract the maximum possible thermal energy from the PEMFC, at the expense of reducing the electrical

efficiency in order to maximize the thermal efficiency, resulting in lower total cost of energy generated. This situation can also be the reverse, in which case it would be worthwhile to maximize the electrical efficiency at the expense of reducing the thermal efficiency. In this regard, taking into account the results obtained, in the best situation the system efficiency could be improved up to 8.91%.

Regarding the economic efficiency, the maximization of it will be determined based on the proportion of energy efficiency optimized by the system optimization control and the different costs of electricity and heat generation, for every moment, between the PEMFC-based CHP system and the auxiliary heat and power generation systems.

It must be taken into account that in this model has not been taken into account the degradation of the internal components of PEMFC-based system. However, it is proposed as a further development of this work, to develop an algorithm that, by performing a power sweep every so often, will be able to readjust the parameters of the neural network and thus contemplate the degradation of the fuel cell stack, thus obtaining more reliable results throughout all the lifetime of the system.

Moreover, it is also proposed for future developments, to take into account certain magnitudes that, during the experimental tests carried out in this work have remained constant and, could also offer some room for improvement in system efficiency. These magnitudes to be taken into account are the following: the ambient temperature, which in this case has been around 20 ° C; the oxygen concentration in the ambient, which in this case has been of 20.6%; the hydrogen supply pressure, which in this case has been of 8 bar; or the relative humidity of the air supplied, which in this case has been of 80%.

5. Conclusions

In this paper has been implemented a model of an integrated PEMFC cogeneration system that is able to emulate the thermal response and the hydrogen consumption of the CHP system to changes in the power and heat demand. The developed model is based on an artificial neural network with a parallel NARX architecture. In order to train the network, experimental tests have been performed with a real PEMFC-based CHP system of 600 W of electrical power.

After training the ANN, the developed model has been tested and validated with experimental data and has been proven to be not only capable of deal with nonlinear multivariate behavior, but also emulates time-dependent behavior of the system modeled quite accurately. The resulting optimal model consists of a parallel architecture feedback-NARX network with two layer: a hidden layer composed of five neurons and an output layer composed of two neurons. A symmetric sigmoid function has been used in the hidden layer, and a linear function in the output layer.

The maximum relative errors obtained when simulating the outlet temperature of cooling system and the hydrogen consumption of the PEMFC-based CHP system have been approximately of 2.98 % and 2.45 %, respectively.

The results obtained have shown that by integrating the optimal model developed in this paper in a control system aimed at maximizing the techno-economic efficiency of a hybrid or grid connected system that includes a PEMFC-based system, the efficiency could be improved up to 8.91%, depending on energy requirements, by giving priority to the maximization of the electrical or thermal efficiency of the PEMFC-based CHP system, based on the generation costs of all devices involved in the system.

Besides, this paper provides the explanation in depth of the methodology used to develop the optimal model obtained. In this sense, anyone who wants to create a black-box model of a different PEMFC-based CHP system and use it to develop efficiency maximization algorithms, to schedule in an optimal way PEMFC-based CHP plants, or to hybridise optimally a PEMFC with other heat and / or power generation technologies, can benefit from the proposed methodology and get results with a substantially good accuracy.

References

[1] A. Arsalis, M.P. Nielsen, and S.K. Kær, "Application of an improved operational strategy on a PBI fuel cell-based residential system for Danish single-family households", *Applied Thermal Engineering*, vol. 50 (1), pp. 704–713, 2013.

[2] O.A. Shaneb, P.C. Taylor, "An evaluation of integrated fuel cell and energy storage systems for residential applications", in IEEE *2009 Proceedings of the 44th International*, pp. 1–5, 2009.

[3] M. Houwing, R.R. Negenborn, M.D. Ilić, and B. Schutter, "Model predictive control of fuel cell micro cogeneration systems", in IEEE *Networking, Sensing and Control. ICNSC '09. International Conference on*, pp. 708–713, 2009.

[4] M. Ceraolo, C. Miulli, and A. Pozio, "Modelling static and dynamic behaviour of proton exchange membrane fuel cells on the basis of electrochemical description", *J. Power Sources*, vol. 113 (1), pp. 131–144, 2003.

[5] X. Kong, A.M. Khambadkone, and S.Y. Thum, "A hybrid model with combined steady-state and dynamic characteristics of PEMFC fuel cell stack", in *Conf. Rec. IAS Annu. Meeting*, pp. 1618–1625, 2005.

[6] S.M. Sharifi, S. Rowshanzamir, M.H. Eikani, "Modelling and simulation of the steady-state and dynamic behaviour of of a PEM fuel cell", Energy, vol. 35 (4), pp. 1633-1646, 2010.

[7] P. Srinivasan, J.E. Sneckenberger, and A. Feliachi, "Dynamic heat transfer model analysis of the power generation characteristics for a proton exchange membrane fuel cell stack", in IEEE *System Theory. Proc. of the 35th Southeastern Symposium on*, pp. 252–258, 2003.

[8] M. Gandiglio, A. Lanzini, M. Santarelli, and P. Leone, "Design and optimization of a proton exchange membrane fuel cell CHP system for residential use", Energy and Buildings, vol. 69, pp. 381–393, 2014.

[9] A. Ferguson and V.I. Urgusal, "Fuel cell modelling for building cogeneration applications", *J. Power Sources*, vol. 113 (1), pp. 30–42, 2004.

[10] M. Shao, X. Zhu, H. Cao, and H. Shen, "An artificial neural network ensemble method for fault diagnosis of proton exchange membrane fuel cell system", Energy, vol. 67, pp. 268-275, 2014.

[11] W.Y. Lee, G.G. Park, T.H. Yang, Y.G. Yoon, and H.S. Kim, "Empirical modeling of polymer electrolyte membrane fuel cell performance using artificial neural networks", *International Journal of Hydrogen Energy*, vol. 29, pp. 961–966, 2004.

[12] S. Jemei, D. Hissel, M.C. Pera, and J.M. Kauffmann, "On-board fuel cell power supply modeling on the basis of neural network methodology", *J. Power Sources*, vol. 124, pp. 479–486, 2003.

[13] N. Yousfi-Steiner, D. Hissel, P. Moçotéguy, D. Candusso, "Diagnosis of polymer electrolyte fuel cells failure modes (flooding & drying out) by neural networks modelling", International Journal of Hydrogen Energy, vol. 36, pp. 3067–3075, 2011.

[14] S. Jemeï, D. Hissel, M.-C. Pera, J.M. Kauffmann, "A new modeling approach of embedded fuel-cell power generators based on artificial neural network", IEEE. Transaction on Industrial Electronics, vol. 55 pp. 437–447, 2008.

[15] N.S. Sisworahardjo, T. Yalcinoz, M.Y. El-Sharkh, M.S. Alam, "Neural network model of 100 W portable PEM fuel cell and experimental verification", International Journal of Hydrogen Energy, vol. 35, pp. 9104–9109, 2010.

[16] K. Chang, "The optimal design for PEMFC modeling based on Taguchi method and genetic algorithm neural networks", International Journal of Hydrogen Energy, vol. 36, pp. 13683–13694, 2011.

[17] A. Saengrung, A. Abtahi, A. Zilouchian, "Neural network model for a commercial PEM fuel cell system", Journal of Power Sources, vol. 172 pp. 749-759, 2007.

[18] W. Lee, G. Park, T. Yang, Y. Yoon, C. Kim, "Empirical modeling of polymer electrolyte membrane fuel cell performance using artificial neural networks", International Journal of Hydrogen Energy, vol. 29, pp. 961-966, 2004.

[19] J. Lobato, P. Cañizares, M.A. Rodrigo, J.J. Linares, C. Piuleac, and S. Curteanu, "The neural networks based modeling of a polybenzimidazole-based polymer electrolyte membrane fuel cell: Effect of temperature", Journal of Power Sources, vol. 192, 99 190-194, 2009.

[20] I.S. Han, H.K. Shin, "Modeling of a PEM fuel cell stack using partial least squares and artificial neural networks", Korean Chem Eng Res, vol. 53, pp. 236–242, 2015.

[21] A.U. Chávez-Ramírez, R. Muñoz-Guerrero, S.M. Durón-Torres, M. Ferrano, G. Brunaccini, F. Sergi, V. Antonucci, and L.G. Arriaga, "High power fuel cell simulator based on artificial neural network", International Journal of Hydrogen Energy, vol. 35, pp. 12125-12133, 2010.

[22] G. Napoli, M. Ferraro, F. Sergi, G. Brunaccini, V. Antonucci, "Data driven models for a PEM fuel cell stack performance prediction", International Journal of Hydrogen Energy, vol. 38, pp. 11628-11638, 2013.

[23] I. Han, S. Park, and C. Chung, "Modeling and operation of a proton exchange membrane fuel cell system for maximum efficiency", Energy Conversion and Management, vol. 113, pp. 52-65, 2016.

[24] A. Vasickaninova, M. Bakosova, A. Mészáros, and J. Jaromir, "Neural network predictive control of heat exchanger", vol. 31 (13), pp. 2094-2100, 2011.

[25] H. Simon, "Neural networks, a comprehensive foundation", 2nd edition, Prentice Hall International Inc., pp. 227-247, 1999.

[26] K.S. Narendra, K. Parthasaranthy, "Identification and Control of Dynamical Systems Using Neural Networks", vol 1 (1), pp. 4-27, 1990.

[27] D.W. Manquardt, "An algorithm for least-squares estimation of nonlinear parameters, Journal of the Society for Industrial and Applied Mathematics", vol. 11 (2), pp. 431-441, 1963.

[28] T. Lin, C.L. Giles, B.G. Horne, and S.Y. Kung, A delay damage model selection algorithm for NARX Neural Networks, IEEE Transactions on Signal Processing, vol. 45 (11), 2719-2730, 1997.

[29] M.T. Hagan, H.B. Demuth, M.H. Beale, and O. De Jesus, "Neural network design", Boston, MA, PWS Publishing, 1996.

[30] C. Wang, S.S. Venkatesh, and J.S. Judd, "Optimal Stoping and Effective Machine Complexity Learning", Advances in Neural Information Processing Systems, Vol. 6, 303-310, 1994.

[31] J. Heaton, "Artificial intelligence for humans, volume 3: Deep Learning and Neural Networks", Heaton Research Inc., 2015.